JACC: CARDIOVASCULAR IMAGING VOL. 14, NO. 8, 2021

ORIGINAL RESEARCH

3D Myocardial Mechanical Wave Measurements

Toward In Vivo 3D Myocardial Elasticity Mapping

Sebastien Salles, PhD,[a] Torvald Espeland, MD,[a,b] Alfonso Molares, PhD,[a] Svein Arne Aase, PhD,[c] Tommy Arild Hammer, MD,[a,d] Asbjørn Støylen, MD,[a] Svend Aakhus, MD,[a,b] Lasse Lovstakken, PhD,[a] Hans Torp, PhD[a]

ABSTRACT

OBJECTIVES This study aimed to investigate the potential of a novel 3-dimensional (3D) mechanical wave velocity mapping technique, based on the natural mechanical waves produced by the heart itself, to approach a noninvasive 3D stiffness mapping of the left ventricle.

BACKGROUND Myocardial fibrosis is recognized as a pathophysiological substrate of major cardiovascular disorders such as cardiomyopathies and valvular heart disease. As fibrosis leads to increased myocardial stiffness, ultrasound elastography measurements could provide important clinical information.

METHODS A 3D high frame rate imaging sequence was implemented on a high-end clinical ultrasound scanner to achieve 820 volumes/s when gating over 4 consecutive cardiac cycles. Five healthy volunteers and 10 patients with various degrees of aortic stenosis were included to evaluate feasibility and reproducibility. Mechanical waves were detected using the novel Clutter Filter Wave Imaging approach, shown to be highly sensitive to the weak tissue displacements caused by natural mechanical waves.

RESULTS 3D spatiotemporal maps of mechanical wave velocities were produced for all subjects. Only the specific mechanical wave at atrial contraction provided a full 3D coverage of the left ventricle (LV). The average atrial kick propagation velocity was 1.6 ± 0.2 m/s in healthy volunteers and 2.8 ± 0.8 m/s in patients ($p = 0.0016$). A high correlation was found between mechanical wave velocity and age ($R^2 = 0.88$, healthy group), septal wall thickness ($R^2 = 0.73$, entire group), and peak jet velocity across the aortic valve ($R^2 = 0.70$). For 3 of the patients, the higher mechanical wave velocity coexisted with the presence of late gadolinium enhancement on cardiac magnetic resonance.

CONCLUSIONS In this study, 3D LV mechanical wave velocities were visualized and measured in healthy volunteers and patients with aortic stenosis. The proposed imaging sequence and measurement technique allowed, for the first time, the measurement of full spatiotemporal 3D elasticity maps of the LV using ultrasound. (Ultrasonic markers for myocardial fibrosis and prognosis in aortic stenosis; NCT03422770) (J Am Coll Cardiol Img 2021;14:1495–505) © 2021 The Authors. Published by Elsevier on behalf of the American College of Cardiology Foundation. This is an open access article under the CC BY-NC-ND license (http://creativecommons.org/licenses/by-nc-nd/4.0/).

From the [a]Centre for Innovative Ultrasound Solutions, Department of Circulation and Medical Imaging, Norwegian University of Science and Technology, Trondheim, Norway; [b]Clinic of Cardiology, St. Olavs Hospital, Trondheim, Norway; [c]GE Vingmed Ultrasound, Trondheim, Norway; and the [d]Clinic of Radiology and Nuclear Medicine, St. Olavs Hospital, Trondheim, Norway.
The authors attest they are in compliance with human studies committees and animal welfare regulations of the authors' institutions and Food and Drug Administration guidelines, including patient consent where appropriate. For more information, visit the Author Center.

Manuscript received December 4, 2019; revised manuscript received April 20, 2020, accepted May 20, 2020.

ISSN 1936-878X https://doi.org/10.1016/j.jcmg.2020.05.037

ABBREVIATIONS AND ACRONYMS

2D = 2-dimensional

3D = 3-dimensional

AKW = atrial kick wave

AS = aortic stenosis

CFWI = clutter filter wave imaging

CMR = cardiac magnetic resonance

ECG = electrocardiogram

HFR = high frame rate

LGE = late gadolinium enhancement

LV = left ventricle

MWV = mechanical wave velocity

SWT = septal wall thickness

V-max = peak jet velocity across the aortic valve using continuous wave Doppler ultrasound

Cardiovascular disease is a leading cause of mortality in the western world (1), and fibrosis is a common pathology in cardiovascular disease (2). In the myocardium, fibrosis leads to electric and mechanical dysfunction (3), and by increasing the myocardial stiffness, both diastolic and systolic function are affected (4). Myocardial fibrosis is associated with a worsened prognosis in many disorders (5,6). Therefore, detection of the amount of fibrosis is essential, as it could have therapeutic implications. Histopathological examination of an endomyocardial biopsy specimen is considered the gold standard for quantifying the extent of myocardial fibrosis, but its invasive nature limits its use. Contrast-enhanced magnetic resonance (CMR) imaging is considered the noninvasive gold standard for detecting fibrosis in the left ventricle (LV) (7), but is cumbersome, expensive, and not bedside available. CMR techniques to evaluate the degree of late gadolinium enhancement (LGE) and extracellular volume have been validated against histological fibrosis (8,9). Using ultrasound imaging, the myocardial reflectivity has been proposed as a marker for LV fibrosis by means of ultrasonic integrated backscatter (10). Strain echocardiography is widely used for assessing myocardial deformation in the evaluation of systolic and diastolic function (11). It has been shown that the passive diastolic deformation patterns correlate to the change in myocardial stiffness during myocardial ischemia; however, the magnitude of passive deformation is load-dependent, and its usefulness as a marker for myocardial stiffness is thus limited.

More recently, shear wave imaging, an ultrasound-based technique for quantitatively mapping the stiffness of soft tissues, was applied with success in an open-chest sheep model (12). Because this technique is based on shear waves produced in ultrasound acoustic radiation force imaging (ARFI), it has the advantage of being able to estimate the stiffness of soft tissue at any time during the cardiac cycle. However, its application remains challenging at cardiac imaging depths due to the fast attenuation of the produced shear wave, limiting its use to only a small part of the myocardium, or open-chest application. Despite these limitations, a few mid-size clinical studies show promising results (13,14).

Instead of ARFI shear waves, natural mechanical waves produced by the body itself can be tracked to estimate and map the stiffness of tissue (15,16). In the LV, several natural waves have been described. Kanai (17,18) first demonstrated time multiple mechanical waves propagating along the septum. One wave was found around the time of the Q-wave of the electrocardiogram (ECG), propagating from the interventricular septum toward both the basal and apical part of the heart with a speed of 1 m/s. This wave was recognized as the propagation of electric activation from the Purkinje fiber-myocyte junction in the interventricular septum and was used for myocardial electric activation mapping (19,20). Other mechanical waves propagating from the base to the apex have been detected at other times in the cardiac cycle and defined as shear waves. One wave originated around the peak of the P-wave in the ECG, propagating with a speed of 1 to 4 m/s (18), and a second wave arose at the time of aortic valve closure and propagated at the same speed (21). The main limitation of the beforementioned technique is the limited region of interest used to characterize the entire LV, as only a small part of the myocardium was studied using a 2-dimensional (2D) view.

The present study investigates the potential of a new high frame rate (HFR) 3-dimensional (3D) acquisition and processing scheme implemented on a high-end clinical scanner to map the mechanical waves naturally produced by the heart for a full 3D stiffness mapping. For reasons given in the following text, this study focus on the specific wave produced at the time of the P-wave, in both healthy subjects and patients.

METHODS

PATIENT MATERIAL. Five healthy volunteers and 10 patients from the clinical study Ultrasonic Markers for Myocardial Fibrosis and Prognosis in Aortic Stenosis (NCT03422770) are presented here. The trial was approved by a Regional Committee for Medical and Health Research Ethics, and all subjects provided informed written consent. The mean age of all the subjects was 64.5 years, and 10 were men. All subjects underwent CMR with the injection of a gadolinium-based contrast agent to evaluate the degree of LGE and extracellular volume.

T_1 mapping was achieved using the MOdified Look-Locker Inversion recovery sequence. Data was recovered in 3 different 8-mm thick short-axis slices at the basal, midventricular and apical levels. Pre- and post-contrast T_1 values were calculated according to recommendations from the American Heart Association, with a 16-segment model. T_1 measurements were achieved in blood and the myocardium before and 10 min after intravenous administration of gadolinium. Using dedicated software (CMR42, Circle

TABLE 1 Patients With Aortic Stenosis With Their CMR Results

ID	Age (yrs)	Sex	Hypertension	V-Max (m/s)*	Symptoms of AS	SWT (mm)†	Native T_1 (ms)‡	LGE on CMR	Extracellular Volume (%)
C1	36	M	No	1.2	No	8.4	1,177 ± 52	No focal areas	22.8 ± 3.6
C2	68	M	No	1.2	No	11.1	1,204 ± 58	No focal areas	24.4 ± 2.6
C3	75	F	No	1.5	No	9.3	1,169 ± 54	No focal areas	22.9 ± 2.5
C4	65	F	No	1.4	No	11.4	1,207 ± 64	No focal areas	27.0 ± 2.8
C5	>80	M	No	1.4	No	11.4	1,197 ± 60	No focal areas	23.6 ± 2.5
P1	69	M	Yes	2.1	No	11.0	1,217 ± 55	No focal areas	24.9 ± 2.7
P2	69	M	Yes	3.5	No	16.0	1,198 ± 48	No focal areas	21.3 ± 2.6
P3	>80	F	No	4.6	Yes	13.0	1,245 ± 73	Yes	22.5 ± 2.9
P4	49	M	Treated previously	4.5	Yes	18.0	1,216 ± 56	No focal areas	23.7 ± 2.1
P5	75	M	No	4.2	Yes	13.9	1,291 ± 55	Yes	27.8 ± 3.9
P6	72	M	No	3.2	No	11.4	1,157 ± 62	No focal areas	25.5 ± 4.9
P7	49	F	No	6.8	Yes	19.0	1,314 ± 51	Yes	27.3 ± 6.2
P8	29	M	No	4.0	No	16.1	1,214 ± 51	No focal areas	23.1 ± 2.4
P9	69	M	No	1.9	No	13.1	1,217 ± 47	No focal areas	Not feasible to calculate
P10	66	F	No	3.5	No	10.6	1,248 ± 63	No focal areas	25.8 ± 5.6

*V-max = Peak jet velocity across the aortic valve. †SWT = Septal wall thickness on CMR. ‡Global value for T_1 = before injection of gadolinium-based contrast agent. LGE = late gadolinium enhancement.

Cardiovascular Imaging, Calgary, Canada), all analyses were done by an experienced CMR reader. The 15 subjects and their CMR findings are briefly presented in Table 1.

The analysis of the conventional echocardiographic data, cardiac magnetic resonance data, and the estimation of the mechanical wave velocities (MWV) were performed by 3 independent and blinded observers (T.E., T.A.H., and S. S.).

3D ULTRASOUND ACQUISITION. The LV of each subject was studied with 2 different 3D acquisitions using a modified Vivid E95 scanner (GE Vingmed Ultrasound, Horten, Norway) and the 4V matrix array probe. The acquisition setup parameters can be found in Table 2. First, a high-quality 3D sequence was acquired for 3D segmentation of the LV. Then, a 3D ultrafast imaging sequence was used for the mechanical wave detection. The 4V probe of E95 does support having a very deep focus. Thus, as long as limited steering is needed, the probe can produce relatively planar transmit waves. The 3D ultrafast imaging sequence was achieved by transmitting 20 of these planar steered waves over 4 cardiac cycles. Upon reception, because E95 has a software beamformer, the number of parallel beams that can be reconstructed varies with the setup used. In this 3D ultrafast imaging setup, 64 receive lines were reconstructed for each transmit. Five planar waves were used for each cardiac cycle to reconstruct 1 part of the LV, at 820 volumes/s. By stitching 4 consecutive cardiac cycles, the whole LV was reconstructed. The ECG stitching has been achieved by detecting the P-wave time. The acquisition time for the entire procedure is 8 s: 6 s for the HFR imaging and 2 s for the high-quality images.

Each acquisition was performed from the apical view with 12 cm imaging depth and 60° sector width by an expert echocardiographer.

MECHANICAL WAVE DETECTION. Mechanical waves were detected using the clutter filter wave imaging (CFWI) approach. CFWI is a new method for detecting mechanical wave propagation without prior motion estimation. The motion of interest, induced by a mechanical wave, is selectively attenuated and thus accentuated by an appropriate wall filter. Thus, the mechanical wave propagation directly appears as darker-intensity regions moving in the B-mode and corresponding anatomic M-mode images. Although only the locality of tissue velocity induced by the mechanical wave is detected, we have shown that the method is more sensitive to subtle tissue displacements when compared to motion estimation

TABLE 2 Acquisition Setup

Speed of sound	1,540 m/s
Transmit center frequency	1.6 MHz
Pulse repetition frequency	4.34 kHz
Number of steered plane waves	5•4
Electrocardiogram stitched	4
Steered plane waves angles (azi × ele)	(−30°,…, 30°) • (−30°,…, 30°)
Imaging volumes	60° • 60° opening angle 200 • 200 lines
Imaging depth	12 cm
View	Apical
Frame rate	820 volumes/s

FIGURE 1 Mechanical Wave of Interest

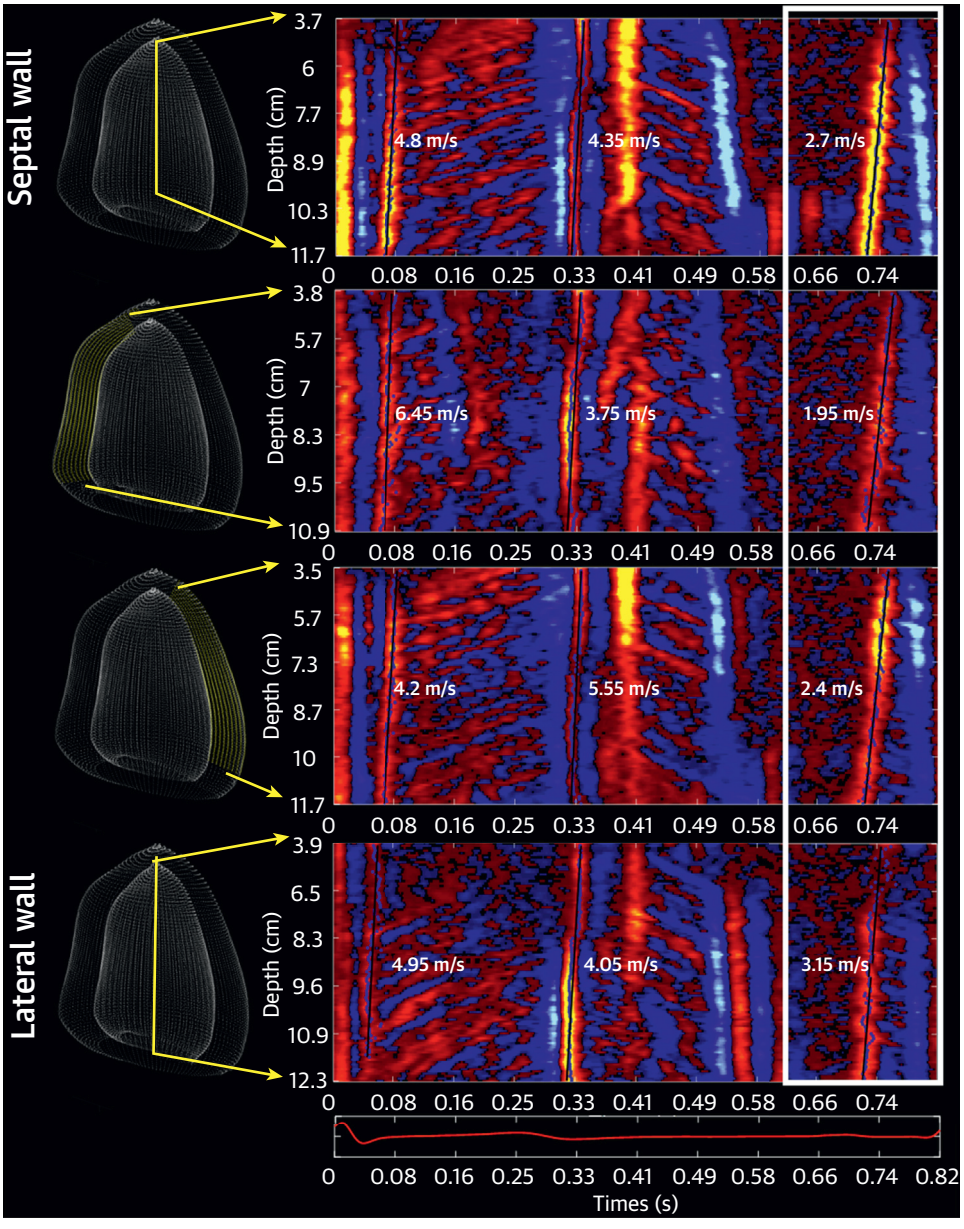

Two-dimensional (2D) spatiotemporal maps obtained with clutter filter wave imaging along 4 anatomic lines. The 4 maps correspond to 4 anatomic lines going from the base to the apex on the septal, anterior, inferior, and lateral wall. The 2D maps were made by taking the average results inside the left ventricular wall **(yellow lines)**. Several mechanical waves were found at different times in the cardiac cycle for each map. The spatiotemporal maps were normalized between 0 and 1. The atrial kick wave is highlighted with a **white box**.

techniques, such as tissue-Doppler. The full process is described previously (22,23). This approach assesses the motion induced by the mechanical wave toward the transducer direction, by assuming that the motion induced by the wave will always have a component in this direction.

MECHANICAL WAVES OF INTEREST. Several mechanical waves were detected at different times in the cardiac cycle (Figure 1). However, only the atrial kick wave (AKW) was detected for all subjects and propagated in the entire LV (Figure 1 white rectangle, Figure 2). Furthermore, this specific wave

CENTRAL ILLUSTRATION **3D Mechanical Wave Velocity Mapping Process**

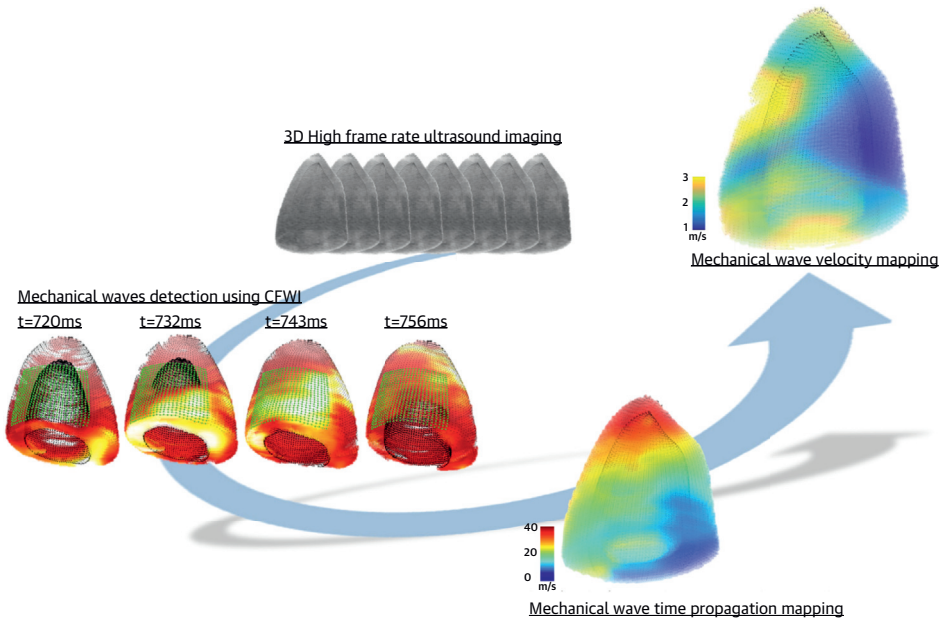

Salles, S. et al. J Am Coll Cardiol Img. 2021;14(8):1495–505.

Mechanical wave mapping using clutter filter wave imaging (CFWI). The time of flight of the mechanical wave velocity (MWV) was estimated by detecting the maximum of the tissue acceleration and mapped on the 3-dimensional (3D) surface of the left ventricle. The local velocities of the mechanical wave were estimated following the method described in the Mechanical Wave Speed Estimation section. The process was repeated in the full volume all around the 3D left ventricular volume, resulting in a 3D display of the mechanical wave velocities.

appears during diastole, at the start of atrial contraction, making it very interesting in several cardiovascular syndromes.

MECHANICAL WAVE SPEED ESTIMATION. The 3D CFWI result represents the axial wall acceleration (along the scanline) of the LV at a specific position. To analyze the measurements, we segmented the myocardium of the 3D LV model from a high-quality 3D B-mode sequence. Thus, the CFWI variation over distance and time could be depicted in a 3D volume corresponding to the myocardium only.

Second, the time of flight of the mechanical wave was estimated by detecting the maximum of the CFWI data, that is, the maximum of the acceleration, which was mapped to the 3D LV volume ($T_{x,y,z}$) (Central Illustration).

Finally, the local MWV was estimated using the following equation:

$$V = \sqrt{\left(\frac{R_x}{\nabla T_x}\right)^2 + \left(\frac{R_y}{\nabla T_y}\right)^2 + \left(\frac{R_z}{\nabla T_z}\right)^2} \qquad \text{(Eq. 1)}$$

where $R_{x,y,z}$ represents the spatial resolution of the 3D LV volume, $T_{x,y,z}$ the time propagation volume, and ∇ the gradient operator. Only the mechanical wave with a positive axial velocity (from the base to the apex) was considered. The estimated velocity inferior or equal to 0 was not considered (white region in Figure 3).

STATISTICAL ANALYSIS. The normality of data was validated using the Shapiro-Wilk test. The coefficient of determination, denoted R^2 was used to evaluate the correlation between the AKW velocity, septal wall thickness (SWT), age, and peak jet velocity across the aortic valve using continuous wave Doppler ultrasound (V-max) and native T_1.

Comparisons between healthy volunteers and patients were performed using a 2-tailed Student's *t*-test assuming unequal variances (Welch). A 2-sided p value of 0.05 was considered statistically significant for all tests.

RESULTS

Figure 1 shows examples of the 2D spatiotemporal maps obtained after CFWI for a healthy subject. These 2D maps were established by averaging radially through the LV wall. The 4 maps correspond to

FIGURE 2 3D Mechanical Wave Visualization

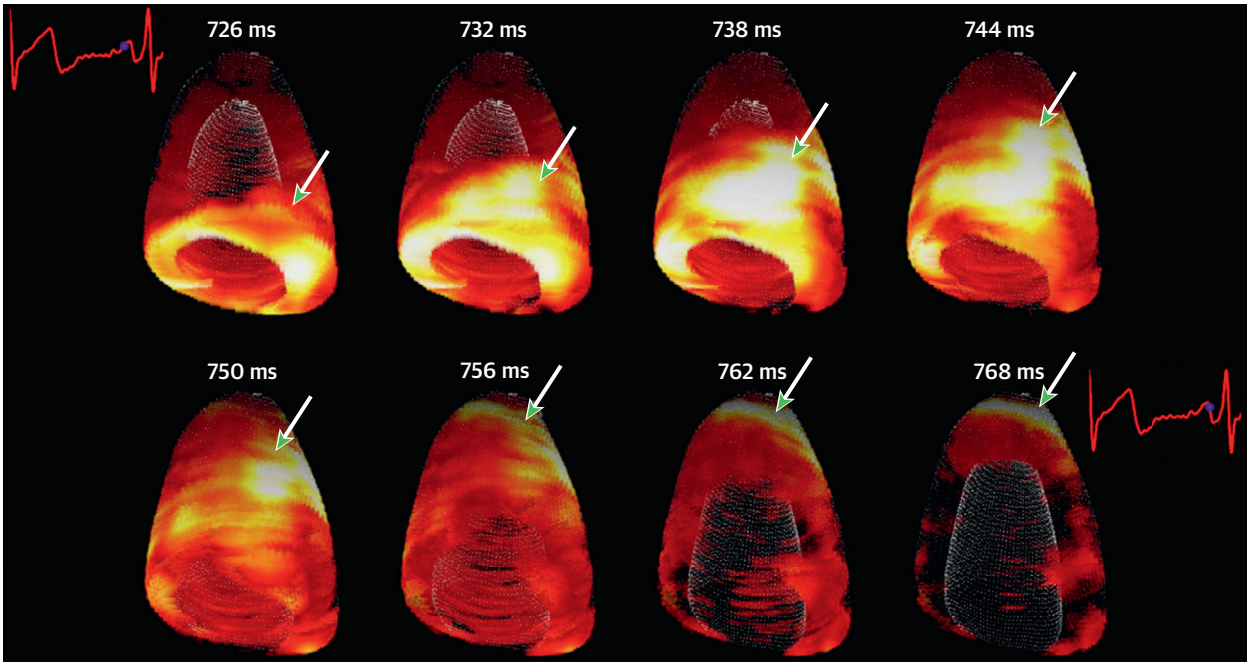

Three-dimensional (3D) visualization of the propagation of the mechanical wave at atrial systole. In healthy subjects, this wave propagates from base to apex at the same time across the entire left ventricular.

4 anatomic lines going from the base to the apex on the septal, anterior, inferior, and lateral wall. The MWV was estimated using a linear regression of the 2D spatiotemporal image maxima (24–26).

Several mechanical waves were detected at different times in the cardiac cycle for each map. The first wave propagating with an average value of 5.0 m/s seems to correspond to the wave produced by the mitral valve closure (19). The second wave propagates at 4.5 m/s and seems to be induced by the aortic valve closure (21). The third wave seems to be induced after the P-wave in the ECG, during the atrial contraction, and propagates with an average velocity of 2.4 m/s. These 3 different waves were found in all the subjects. However, whereas the different mechanical waves were detectable, only the AKW was detected for all the subjects and propagated throughout the entire LV.

The 3D propagation of this specific wave is shown in **Figure 2**. We noticed that this wave starts to propagate from base to apex approximately at the same time all around the LV. The **Central Illustration** shows the 3D MWV mapping process. After the detection of the mechanical wave of interest with CFWI, the local velocity estimates of the mechanical wave were 3D mapped following the method described in the Mechanical Wave Speed Estimation section.

To simplify interpretation, the bullseye view is used to present these results. Bullseye plots of the estimated AKW velocity for all the subjects are displayed in **Figure 3**. The average value corresponding to the basal, mid, and apical region is given under each plot. The average AKW velocity was 1.6 ± 0.2 m/s in healthy volunteers and 2.8 ± 0.8 m/s in patients ($p = 0.0016$) (**Figure 4**). For all healthy subjects, the averaged estimated AKW velocities was higher in the base than in the apex.

Patients P1, P2, and P10 showed similar AKW velocities as the 5 healthy subjects (around 2.0 m/s). The rest of the patients demonstrated an AKW velocity >2.5 m/s, possibly indicating a stiffer heart. Four of these 7 patients had severe symptomatic aortic stenosis (AS), and 3 of them displayed LGE on CMR (**Table 2**).

A positive and high correlation was found between AKW velocity and SWT ($R^2 = 0.73$) (**Figure 5B**), and between the AKW velocity and V-max ($R^2 = 0.70$) (**Figure 5C**). A weak correlation was found between

FIGURE 3 **Bullseye Plot of 3D Mechanical Wave Mapping-Healthy Subjects and Patients**

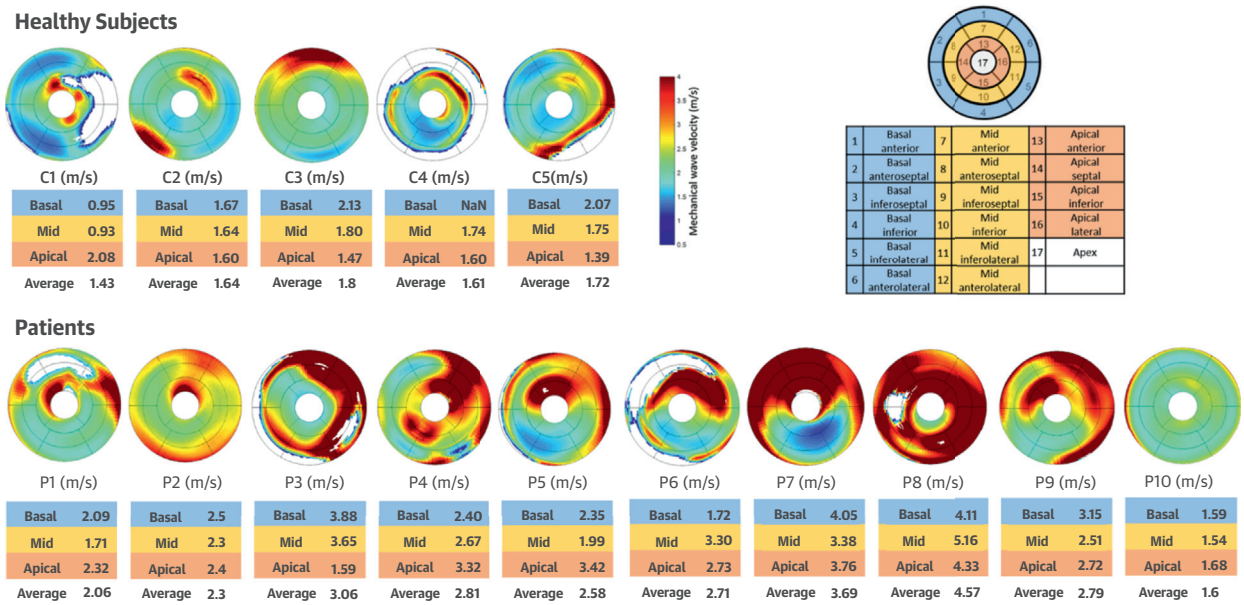

Bullseye plot of the estimated atrial kick wave velocities, for the 5 healthy subjects and 10 patients with aortic stenosis (AS). The average value was depicted under each plot. The estimated velocities were between 0.9 and 2.1 m/s for control subjects and between 1.5 and 5.2 for patients. The missing regions **(white region)** corresponds to axial velocities inferior or equal to 0.

the AKW velocity and native T_1 ($R^2 = 0.33$) (Figure 5D). No correlation was found between the extracellular volume and the AKW velocity.

DISCUSSION

The detection of the amount of fibrosis is essential for many myocardial disorders (5,6). CMR is considered the noninvasive gold standard for detecting fibrosis in the LV (7). Furthermore, MR elastography have also demonstrated some potential in the evaluation of myocardial stiffness (26). However, cardiac magnetic resonance remains less available, is more expensive, and compared with echocardiography, comes with some contraindications and potential discomfort. In this paper, the feasibility of full 3D mechanical wave mapping using "natural" mechanical waves produced by the heart itself was demonstrated, with the aim to quantify myocardial stiffness.

The recordings were done using a high-end clinical ultrasound system with a 4V matrix array transducer. A special high frame rate 3D imaging setup was developed, using 20 unfocused ultrasound pulses to cover the full LV volume. In addition, a new method, CFWI, was employed for detecting and estimating the mechanical waves. Methods such as speckle tracking or tissue-Doppler have previously been used for the estimation of the axial displacement induced by mechanical waves, but CFWI provides more robust detection of small tissue perturbations, which is essential due to the reduced image quality and penetration of HFR imaging sequences. In this work, the method proved able to detect several mechanical waves with sufficient quality for subsequent velocity estimation. By tuning the settings of CFWI carefully, even better results might be obtained. In this initial study, we chose to apply the same parameter setup for all subjects.

Several other events were detected at different times in the cardiac cycle. Two of them were visible, for example, 0.4 and 0.5 s after the start of the R-wave in the ECG (Figure 1). Although these events were detected in all subjects, the estimated velocities were not within expected values, and potentially does not represent mechanical waves.

The trigger and the nature of the specific mechanical wave under investigation is still unknown. We therefore chose to report the wave velocity, and not compute the stiffness of the tissue through a corresponding constitutive equation. However, different hypotheses could be proposed. First, we

FIGURE 4 AKW Velocity Healthy Volunteers Versus Patients

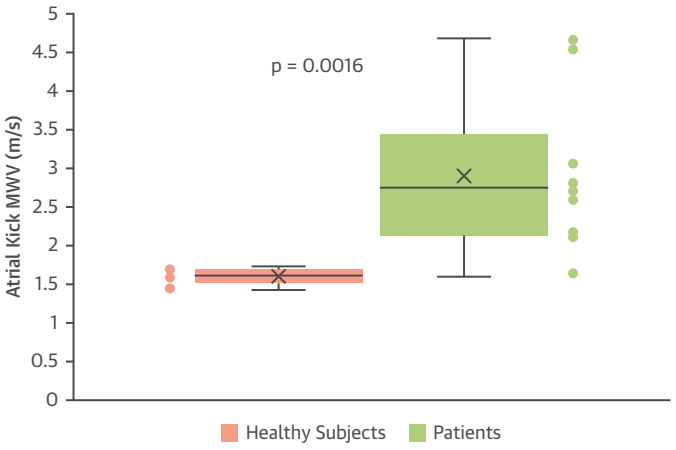

Comparison of average atrial kick wave velocity in healthy volunteers **(green)** and patients with AS **(red)**. On each **box**, the **central mark** indicates the average, the **cross** indicates the median, and the **bottom and top edges of the box** indicate the 25th and 75th percentiles, respectively. The **whiskers** extend to the most extreme data points. The **dots** correspond to the individual results. MWV = mechanical wave velocity.

could argue that it is a shear wave, similar to the wave produced by the closing aortic valve. In this case, the relationship to the stiffness is straightforward using the following equation:

$$\mu = \rho c^2 \qquad \text{(Eq. 2)}$$

Where c is the shear wave velocity in m/s, ρ is the density of the tissue in kg/m^3, and μ the shear modulus in Pa (i.e., stiffness). However, contrary to the aortic valve closure wave, the studied wave does not seem to attenuate with time, and it propagates throughout the entire LV. A second hypothesis could be that the detected wave is the electromechanical wave that appears during the P-wave. In this case, the propagation of the wave should originate from the middle of the septum, and propagate toward the apex and then further down the lateral wall. From what we observed, the direction of propagation differs from the electric conduction system. Indeed, the wave propagates uniformly from the base to the apex of the LV. This observation leads us to a third hypothesis. In the manner of a pulse wave propagating in the artery (15), the detected wave could be a pressure wave propagating inside the LV, inducing the detected motion on the walls. This hypothesis is supported by the fact that this wave is produced and propagates during atrial systole, where a variation of the intraventricular pressure is expected. Thus, the pressure propagation inside the ventricle may induce the myocardial stretch propagation previously described (27,28) where similar velocity propagation has been reported. In that scenario, the wall thickness and the radius of the LV must be taken into account in addition to the LV diastolic pressure to estimate myocardial stiffness. Finally, the studied motion pattern could also reflect the propagation of myocardial contraction. The AKW velocities were similar for most of the healthy subjects, with an average value of 1.6 ± 0.2 m/s, in agreement with previously reported values (18). Moreover, in the healthy volunteers, the estimated AKW velocity was higher in the basal region than in the apex. This can be interpreted as a stiffer myocardium in the base. If so, this result might be explained by the fibrotic ring present at the base of the LV (29–31).

Concerning the 10 patients, 3 had similar average MCVs as the healthy volunteers, and 7 had an average AKW velocity >2.5 m/s ($p = 0.005$), which could indicate an overall stiffer LV. When comparing these results to the MR findings shown in **Table 1**, the higher AKW velocity of the 3 patients (P3, P5, and P7) could be explained by fibrotic tissue. For the 4 remaining patients (P4, P6, P8, and P9), no signs of LGE was detected. Note that focal LGE is only indicative of local and not diffuse fibrosis. Moreover, positive correlation was detected between AKW velocity and SWT measured with CMR ($R^2 = 0.73$) (**Figure 5B**). Myocardial wall thickness is often increased in patients with myocardial fibrosis (32,33).

The presented method has some limitations related to the acquisition scheme and clinical feasibility. Currently, the HFR sequences were recorded using 4 cardiac cycles for the mechanical wave mapping, and an additional 1 to 2 cycles to obtain high-quality 3D B-mode images. The separate high-quality B-mode acquisition was needed to properly segment the LV when creating the 3D map. Furthermore, to obtain a full 3D map, the acoustic window must allow for the full LV in 1 recording. Moreover, the reduced signal-to-noise ratio of HFR recordings can potentially make the estimation of tissue velocities challenging at higher depths. In particular, the small perturbations resulting from the mechanical wave sources might be affected. This remains to be investigated. The AKW velocity has been used as “marker” of the tissue stiffness. However, the nature of the AKW remains to be fully understood. Other parameters, such as left ventricle geometry, wall thickness, and loading conditions may influence the AKW velocity, as well as the myocardial stiffness.

FIGURE 5 **Atrial Kick Wave Velocities Versus Age, SWT, V-Max and Native T1**

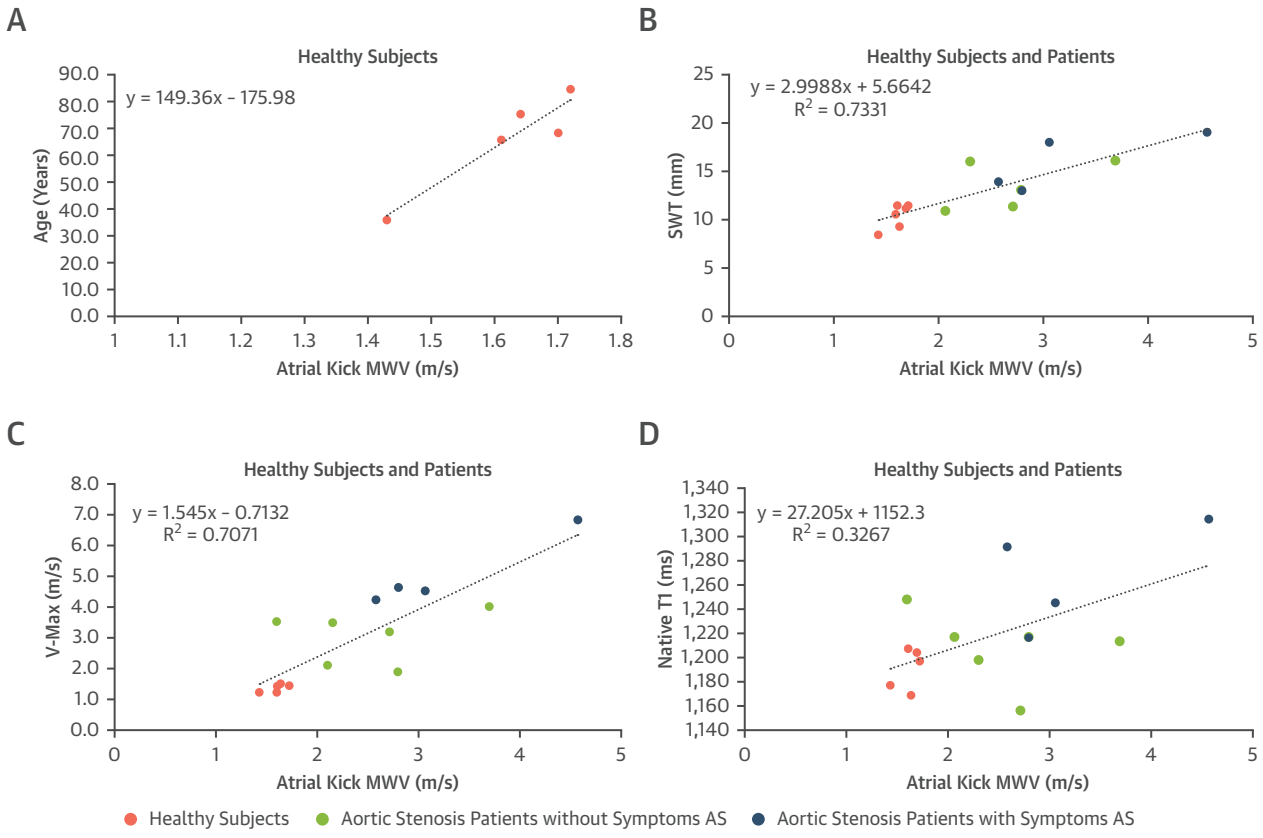

Linear regression analysis between the AKW velocities and age, SWT, V-max, and native T_1. A high correlation was found with V-max ($R^2 = 0.70$) and SWT ($R^2 = 0.73$). AKW = atrial kick wave; MWV = mechanical wave velocity; SWT = septal wall thickness; V-max = peak jet velocity across the aortic valve.

In this work, only the magnitude of the AKW velocity has been used to characterize the tissue stiffness. However, the AKW trajectory related to the AKW velocity vector orientation could be studied and will be in future work.

CLINICAL APPLICATION. The presented method could be used for the detection of diseases leading to a change in myocardial stiffness, such as scars from ischemic disease or fibrosis from any origin. Additionally, in the current European guidelines for valvular heart disease, the evaluation of myocardial fibrosis is mentioned as a mean of providing additional prognostic information in patients with AS (34). Myocardial stiffness will influence the propagation velocity of mechanical waves produced physiologically by the heart itself. In this work, we measured and report the velocities of these waves, whereas calibrated stiffness values may require knowledge of the tissue boundary conditions. A clinically approved ultrasound system was used to acquire the data, and the method can be made bedside applicable. From the 3D velocity map, a global average can be extracted to characterize the global value of fibrotic stages, while the regional value, for instance, can be used to localize scars following infarction. However, the nature of the AKW remains to be fully understood, and further clinical investigation and validation is needed before this marker is ready for clinical use.

STUDY LIMITATIONS. The current study was limited to 5 healthy volunteers and 10 patients with AS and served as an initial demonstration of the feasibility of this new method. Uncertainties can be attributed to both the HFR imaging sequence as well as the estimation of AKW velocities. As a continuation of this work, a study must be conducted to assess the clinical feasibility and to establish normal values in a larger population. In addition, the potential clinical utility

must be documented and further compared to current and relevant measurements, such as deformation analysis (i.e., strain). Moreover, the material properties in the LV are probably the result of interplay of more factors. One such is the diastolic pressure, which may influence stiffness and thus the kick wave propagation.

CONCLUSIONS

In this study, we quantitatively assessed the velocities of the mechanical waves naturally produced by the heart in healthy volunteers and patients with AS. For the first time, the 3D mapping of these velocities was achieved using a custom HFR 3D acquisition scheme. A particularly interesting wave was found during atrial contraction, propagating throughout the LV from the base to the apex. A good correlation was found with age ($R^2 = 0.88$, healthy group), and SWT ($R^2 = 0.73$, entire group). The estimated AKW velocity was found to be between 1.0 and 2.1 m/s for the healthy subjects and between 1.5 and 5.5 m/s for the patients. In 3 of the subjects, the higher AKW velocity was accompanied by the presence of LGE on CMR. The ability of the presented method to detect cardiac disease remains to be demonstrated in further clinical studies.

FUNDING SUPPORT AND AUTHOR DISCLOSURES

This work was supported by CIUS (Centre for Innovative Ultrasound Solutions), a center for Research-based Innovation, supported by the Research Council of Norway. Dr. Lovstakken has served as a consultant with GE Vingmed Ultrasound AS. Dr. Aase has served as an employee of GE Vingmed Ultrasound AS. All other authors have reported that they have no relationships relevant to the contents of this paper to disclose.

ADDRESS FOR CORRESPONDENCE: Dr. Sébastien Salles, Department of Circulation and Medical Imaging, Norwegian University of Science and Technology, 16 rue du general, Guilhem, 75011 Paris, France. E-mail: sebastien.salles@ntnu.no.

PERSPECTIVES

COMPETENCY IN MEDICAL KNOWLEDGE: The evaluation of myocardial stiffness can be a determinant for the detection of myocardial diseases and associated mortality. However, the detailed link between these aspects remains largely unknown, and noninvasive fibrosis imaging could help provide new medical knowledge in this domain.

TRANSLATIONAL OUTLOOK: Despite promising results of shear wave imaging to estimate tissue stiffness in other clinical applications, the estimation of myocardial stiffness noninvasively remains challenging. The quantitative estimation of the propagation velocity of naturally occurring mechanical waves could be a promising alternative to evaluate regional and global myocardial stiffness. Being able to detect myocardial stiffness without the use of CMR and histopathology would have great clinical benefit. Noninvasive evaluation of myocardial stiffness by imaging the natural mechanical waves by ultrasound needs further clinical validation. A larger clinical study is ongoing, and should provide more answers.

REFERENCES

1. Townsend N, Wilson L, Bhatnagar P, Wickramasinghe K, Rayner M, Nichols M. Cardiovascular disease in Europe: epidemiological update 2016. Eur Heart J 2016;37:3232–45.

2. Rockey DC, Bell PD, Hill JA. Fibrosis—a common pathway to organ injury and failure. N Engl J Med 2015;372:1138–49.

3. Burstein B, Nattel S. Atrial fibrosis: mechanisms and clinical relevance in atrial fibrillation. J Am Coll Cardiol 2008;51:802–9.

4. Kass DA. What mechanisms underlie diastolic dysfunction in heart failure? Circ Res 2004;94:1533–42.

5. Barison A, Grigoratos C, Todiere G, Aquaro GD. Myocardial interstitial remodelling in non-ischaemic dilated cardiomyopathy: insights from cardiovascular magnetic resonance. Heart Fail Rev 2015;20:731–49.

6. Azevedo CF, Nigri M, Higuchi ML, et al. Prognostic significance of myocardial fibrosis quantification by histopathology and magnetic resonance imaging in patients with severe aortic valve disease. J Am Coll Cardiol 2010;56:278–87.

7. Iles L, Pfluger H, Phrommintikul A, et al. Evaluation of diffuse myocardial fibrosis in heart failure with cardiac magnetic resonance contrast-enhanced T1 mapping. J Am Coll Cardiol 2008;52:1574–80.

8. Flett AS, Hayward MP, Ashworth MT, et al. Equilibrium contrast cardiovascular magnetic resonance for the measurement of diffuse myocardial fibrosis: preliminary validation in humans. Circulation 2010;122:138–44.

9. Messroghli DR, Moon JC, Ferreira VM, et al. Clinical recommendations for cardiovascular magnetic resonance mapping of T1, T2, T2* and extracellular volume: A consensus statement by the Society for Cardiovascular Magnetic Resonance (SCMR) endorsed by the European Association for Cardiovascular Imaging (EACVI). J Cardiovasc Magn Reson 2017;19:75.

10. Prior DL, Somaratne JB, Jenkins AJ, et al. Calibrated integrated backscatter and myocardial fibrosis in patients undergoing cardiac surgery. Open Heart 2015;2:e000278.

11. Pislaru C. Ultrasound strain imaging of altered myocardial stiffness: stunned versus infarcted reperfused myocardium. Circulation 2004;109:2905–10.

12. Pernot M, Lee W-N, Bel A, et al. Shear wave imaging of passive diastolic myocardial stiffness: Stunned versus infarcted myocardium. J Am Coll Cardiol Img 2016;9:1023–30.

13. Song P, Bi X, Mellema DC, et al. Quantitative assessment of left ventricular diastolic stiffness using cardiac shear wave elastography: a pilot study. J Ultrasound Med 2016;35:1419–27.

14. Villemain O, Correia M, Mousseaux E, et al. Myocardial stiffness evaluation using noninvasive

shear wave imaging in healthy and hypertrophic cardiomyopathic adults. J Am Coll Cardiol Img 2019;12:1135–45.

15. Vappou J, Luo J, Konofagou EE. Pulse wave imaging for noninvasive and quantitative measurement of arterial stiffness in vivo. Am J Hypertens 2010;23:393–8.

16. Apostolakis IZ, Nandlall SD, Konofagou EE. Piecewise pulse wave imaging (pPWI) for detection and monitoring of focal vascular disease in murine aortas and carotids in vivo. IEEE Trans Med Imaging 2016;35:13–28.

17. Kanai H. Propagation of spontaneously actuated pulsive vibration in human heart wall and in vivo viscoelasticity estimation. IEEE Trans Ultrason Ferroelectr Freq Control 2005;52:1931–42.

18. Kanai H. Propagation of vibration caused by electrical excitation in the normal human heart. Ultrasound Med Biol 2009;35:936–48.

19. Konofagou EE, Provost J. Electromechanical wave imaging for noninvasive mapping of the 3D electrical activation sequence in canines and humans in vivo. J Biomech 2012;45:856–64.

20. Provost J, Lee W-N, Fujikura K, Konofagou EE. Imaging the electromechanical activity of the heart in vivo. Proc Natl Acad Sci U S A 2011;108:8565–70.

21. Vos HJ, van Dalen BM, Heinonen I, et al. Cardiac shear wave velocity detection in the porcine heart. Ultrasound Med Biol 2017;43:753–64.

22. Salles S, Aase SA, Bjastad T, Lovstakken L, Torp H. Clutter Filter Wave Imaging (CFWI): A New Way to Visualize and Detect Mechanical Waves Propagation. 2017 IEEE International Ultrasonics Symposium (IUS). Washington, DC: IEEE; 2017.

23. Salles S, Lovstakken L, Aase SA, Bjastad TG, Torp H. Clutter filter wave imaging. IEEE Trans Ultrason Ferroelect Freq Contr 2019;66:1444–52.

24. Santos P, Petrescu AM, Pedrosa J, et al. Natural shear wave imaging in the human heart: normal values, feasibility, and reproducibility. IEEE Trans Ultrason Ferroelect Freq Contr 2019;66:442–52.

25. Petrescu A, Santos P, Orlowska M, et al. Velocities of naturally occurring myocardial shear waves increase with age and in cardiac amyloidosis. J Am Coll Cardiol Img 2019;12:2389–98.

26. Khan S, Fakhouri F, Majeed W, Kolipaka A. Cardiovascular magnetic resonance elastography: a review. NMR Biomed 2018;31:e3853.

27. Voigt J-U, Lindenmeier G, Werner D, et al. Strain rate imaging for the assessment of preload-dependent changes in regional left ventricular diastolic longitudinal function. J Am Soc Echocardiogr 2002;15:13–9.

28. Pislaru C, Alashry MM, Thaden JJ, Pellikka PA, Enriquez-Sarano M, Pislaru SV. Intrinsic wave propagation of myocardial stretch, a new tool to evaluate myocardial stiffness: a pilot study in patients with aortic stenosis and mitral regurgitation. J Am Soc Echocardiogr 2017;30:1070–80.

29. Nagata Y, Wu VC-C, Otsuji Y, Takeuchi M. Normal range of myocardial layer-specific strain using two-dimensional speckle tracking echocardiography. PLoS ONE 2017;12:e0180584.

30. Leitman M, Lysyansky P, Sidenko S, et al. Two-dimensional strain–a novel software for real-time quantitative echocardiographic assessment of myocardial function. J Am Soc Echocardiogr 2004;17:1021–9.

31. Eek C, Grenne B, Brunvand H, et al. Strain echocardiography predicts acute coronary occlusion in patients with non-ST-segment elevation acute coronary syndrome. Eur J Echocardiogr 2010;11:501–8.

32. Méndez C, Soler R, Rodríguez E, et al. Differential diagnosis of thickened myocardium: an illustrative MRI review. Insights Imaging 2018;9:695–707.

33. Pujadas S, Carreras F, Arrastio X, et al. Detection and quantification of myocardial fibrosis in hypertrophic cardiomyopathy by contrast-enhanced cardiovascular magnetic resonance. Revista Española de Cardiología (English Edition) 2007;60:10–4.

34. Baumgartner H, Falk V, Bax JJ, et al. 2017 ESC/EACTS guidelines for the management of valvular heart disease. Eur Heart J 2017;38:2739–91.

KEY WORDS left ventricle, natural mechanical wave, stiffness mapping, 3D ultrasound high frame rate imaging